The Miami2001 Infrared Radiometer Calibration and Intercomparison. Part I: Laboratory Characterization of Blackbody Targets

J. P. RICE,* J. J. BUTLER,+ B. C. JOHNSON,* P. J. MINNETT,# K. A. MAILLET,# T. J. NIGHTINGALE,@ S. J. HOOK,& A. ABTAHI,& C. J. DONLON,** AND I. J. BARTON++

*Optical Technology Division, National Institute of Standards and Technology, Gaithersburg, Maryland
+NASA Goddard Space Flight Center, Greenbelt, Maryland
#Division of Meteorological and Physical Oceanography, Rosenstiel School of Marine and Atmospheric Science, University of Miami, Miami, Florida
@Space Science and Technology Department, Rutherford Appleton Laboratory, Chilton, Didcot, Oxfordshire, United Kingdom
&Jet Propulsion Laboratory, California Institute of Technology, Pasadena, California
**European Commission Joint Research Centre, Institute for Environment and Sustainability, Inland and Marine Water Unit, Ispra, Italy
++CSIRO Marine Research, Hobart, Tasmania, Australia

(Manuscript received 30 September 2002, in final form 5 June 2003)

ABSTRACT

The second calibration and intercomparison of infrared radiometers (Miami2001) was held at the University of Miami's Rosenstiel School of Marine and Atmospheric Science (RSMAS) during May–June 2001. The participants were from several groups involved with the validation of skin sea surface temperatures and land surface temperatures derived from the measurements of imaging radiometers on earth observation satellites. These satellite instruments include those currently on operational satellites and others that will be launched within two years following the workshop. There were two experimental campaigns carried out during the 1-week workshop: a set of measurements made by a variety of ship-based radiometers on board the Research Vessel *F. G. Walton Smith* in Gulf Stream waters off the eastern coast of Florida, and a set of laboratory measurements of typical external blackbodies used to calibrate these ship-based radiometers. This paper reports on the results obtained from the laboratory characterization on blackbody sources. A companion paper reports on the at-sea measurements. Five blackbody sources were intercompared by measurements of their brightness temperature using the National Institute of Standards and Technology (NIST) Thermal-infrared Transfer Radiometer (TXR). Four of these sources are used for calibration of sea surface temperature radiometers. The fifth was a NIST water bath blackbody used for calibration of the TXR. All blackbodies agreed to better than ± 0.1°C at blackbody temperatures near the ambient room temperature. Some of the blackbodies had reduced effective emissivity relative to the NIST water bath blackbody, and hence they began to disagree at blackbody temperatures far enough away (>15°C) from the ambient room temperature. For these, relative effective emissivity values were determined so that corrections can be applied if they are used in conditions of nonlaboratory ambient temperatures.

1. Introduction

Radiometers used to measure skin sea surface temperature and land surface temperature often require calibration with uncertainties approaching 0.1°C or below. The absolute calibration of such radiometers is generally accomplished through a series of measurements where the radiometer views a source of known brightness temperature. One common type of source in use by the sea surface temperature validation community is the cavity blackbody, which can be easily and inexpensively fabricated by most groups. What is more difficult and costly is the development of a full uncertainty analysis based on experimental characterization of the actual components used for these sources. Generally this is only carried out in a partial sense, replacing experimental characterizations with assumptions. For example, while an International System of Units (SI)-traceable thermometer is used, it measures the temperature only at one point and various assumptions about temperature gradients are usually made since full characterization of temperature gradients across all surfaces of the cavity blackbody actually used is usually not possible. In particular, the thermal gradient normal to the surface of the cavity, across the thickness of the cavity coating, is difficult to measure. Also, measurements of the emissivity of blackbody cavity coatings are usually performed on flat witness samples: not on the cavity itself as it is used. Hence assumptions must be made that imperfections accumulated during normal practical use,

Corresponding author address: J. P. Rice, Optical Technology Division, NIST, 100 Bureau Dr., Mail Stop 8441, Gaithersburg, MD 20899.
E-mail: joe.rice@nist.gov

such as dust accumulation, residue from condensation, or sea salt spray, do no affect the measurements at the level of uncertainty required. While the assumptions are usually reasonable, an experimental verification of the resulting brightness temperature scale placed on such blackbodies is warranted in order to verify the low assigned uncertainties. This paper presents the results of such an experimental verification.

The experiments took place as part of the second calibration and intercomparison of infrared radiometers (Miami2001) workshop that was held at the University of Miami's Rosenstiel School of Marine and Atmospheric Science (RSMAS) during May–June 2001 (Barton et al. 2004, hereafter Part II, this issue). In addition to the laboratory-based measurements reported here, there were ship-based measurements performed during this workshop, as detailed in Part II.

The method employed was to use an ultrastable, well-characterized filter radiometer [the National Institute of Standards and Technology (NIST) Thermal-infrared Transfer Radiometer (TXR); Rice and Johnson (1998)] in reasonably controlled laboratory conditions to view several cavity blackbodies and measure the brightness temperature of each. It was a spot-check only, in that it was limited to the field of view, the spectral bands, background loading, etc. offered by the particular filter radiometer used, which did not match those of the ship-based radiometers exactly. However, these parameters were all within the range where the scale for any participating blackbody should be valid. That is, no corrections to the contact temperature are made by any of the users of the participating blackbodies in placing a brightness temperature scale on their blackbodies, which they use for calibration of the ship-based radiometers. Thus, any small radiometer-dependent effects that could arise from field-of-view, emissivity, or background loading have already been ignored (or lumped into the uncertainty) by the blackbody users, justifying the use of other types of radiometers for intercomparisons.

2. The blackbody sources

For the laboratory intercomparison of blackbodies, there was one reference blackbody, the NIST water bath blackbody (WBBB), and four other participating blackbodies (BBs): The RSMAS BB, the Jet Propulsion Laboratory (JPL) BB, the Combined Action for the Study of the Ocean Thermal Skin (CASOTS) Rutherford Appleton Laboratory (RAL) BB, and the CASOTS Southampton Oceanography Centre (SOC) BB. All of these were operated independently of each other in the same laboratory at RSMAS during the workshop. Each BB consisted of a conical metal cavity with a black coating on the inside and each was surrounded on the outside by its own stirred fluid bath to improve temperature uniformity. They each had a calibrated thermometer located in the stirred bath, which was used to determine the temperature of the cavity. All cavity exit apertures were of the order of 10 to 11 cm in diameter, and all BBs were designed to be horizontally emitting. Beyond these general similarities, these five BBs can be classified into two groups depending on whether the bath temperature has active control or not. The NIST WBBB and the RSMAS BB have active temperature control of the bath and essentially follow a design described previously (Fowler 1995). The JPL BB, the CASOTS RAL BB, and the CASOTS SOC BB do not have active temperature control and follow another general design described previously (Donlon et al. 1999; note: there is an error in this paper on page 1189, section d, paragraph 2, in the statement ''and the data presented here were collected at 283 K. The temperature of the NIST BB was allowed to stabilize at 283 K before the MAERI began collecting data. . .''. The mistake is that the values reported as 283 K should have been reported as being at 303.15 K.).

The WBBB and the RSMAS BB are each built into modified Hart Scientific[1] temperature-regulated baths (Fowler 1995). In this design, the copper cavity is mounted into a hole cut into one end of the bath housing. These baths include a fluid stirrer to maintain temperature uniformity, and a refrigerator and heater for controlling the temperature of the fluid bath to within a stability of ± 0.001°C over indefinitely long periods. Each bath includes a thermistor that is the in-loop sensor used for temperature control, and a second, out-of-loop temperature sensor that is calibrated to high accuracy and used for fluid bath temperature measurements. As the bath temperature gradients measured on a blackbody of this type have been measured to be on the order of 0.01°C or less (Fowler 1995), no correction is applied for temperature gradients and the temperature measured by this out-of-loop sensor is taken as the cavity thermodynamic temperature.

NIST fabricated and coated the WBBB cavity and performed its assembly in the WBBB bath. It has been in use at NIST for a number of years. Prior to shipping the WBBB to the RSMAS workshop, the NIST thermometry group recalibrated the out-of-loop temperature sensor, a standard platinum resistance thermometer (SPRT, Rosemount model 162CE), against the ITS-90, and calibrated the Hart Scientific Model 1575 readout electronics for this SPRT to read the SPRT resistance accurately at the triple point of water. Deionized water was used as the fluid for the WBBB.

RSMAS had Hart Scientific fabricate and coat the RSMAS BB cavity and perform the assembly. A diluted solution of ethylene glycol–based antifreeze was used as the fluid for the RSMAS BB, as is the common prac-

[1] References are made to certain commercially available products in this paper in order to adequately specify the experimental procedures involved. Such identification does not imply recommendation or endorsement by the National Institute of Standards and Technology, nor does it imply that these products are the best for the purpose specified.

TABLE 1. Black paints used to coat the cavities of the blackbodies tested.

Blackbody	Type of paint
NIST WBBB	Testors black gloss model paint 1147
RSMAS BB	Testors gloss enamel black paint 61147
JPL BB	Testors gloss enamel black paint 61147
CASOTS RAL BB	Nextel velvet 811-21
CASOTS SOC BB	Nextel velvet 811-21

tice during use of the RSMAS BB for calibration of sea surface temperature radiometers.

To enable the calibrations and aperture reduction tests described later, three auxiliary apertures having opening diameters of 5, 4, and 2.5 cm were used. These apertures fit onto the front of the 11-cm exit aperture of the cavities of the RSMAS BB and NIST WBBB in a manner whereby they can be placed or removed rapidly and repeatably. They are gold coated on the surface facing back into the BB, which increases the effective cavity emissivity. They are painted with a diffuse black paint (MH2200) on the surface facing the radiometer, which reduces scattered light. They also include tapered edges to minimize the amount of scattered light.

The JPL BB, the CASOTS RAL BB, and the CASOTS SOC BB were each built into modified commercial insulated rectangular plastic coolers (Donlon et al. 1999). In this design the metal cavity is mounted into a hole cut into the side of the cooler. Water was used as the bath fluid for these three blackbodies, and a large volume water pump directed the flow along the cavity axis to maintain spatial uniformity. Bath temperatures below ambient room temperature were achieved by adding ice to the water bath, waiting for it to melt, and letting the water bath reestablish a uniform temperature. The bath was warmed as required using an electrical heater. The JPL cavity differs slightly in size from that used in the CASOTS BBs. Otherwise they were similar in construction.

The types of black paint used to coat the inside of the BB cavities are listed for reference in Table 1. While paint type is certainly one factor that determines the cavity effective emissivity, it is not the only one. The thickness, which depends on the application method, the substrate, and the material thermal properties also play a role. For example, the thickness determines the level of thermal gradients across the coating.

3. The NIST TXR

The TXR is a two-channel, liquid nitrogen–cooled, portable filter radiometer. Details of the TXR have been described previously (Rice and Johnson 1998). Channel 1 is centered at 5 μm and has a nominal bandwidth of 1 μm. Channel 2 is centered at 10 μm and has a nominal bandwidth of 1 μm. It has a full field of view of 30 mrad. The TXR can operate in either an ambient mode or chamber mode. In both cases the TXR mirrors, baffles, apertures, detectors, preamplifiers, dichroic beamsplitter, bandpass filters, and tuning fork chopper are all in a sealed-off vacuum and cooled to near 77 K via contact with an internal liquid nitrogen dewar that is part of the TXR cryostat. In ambient mode the TXR cryostat case, including the ZnSe cryostat window, is near room temperature in an ordinary laboratory environment, as shown in Fig. 1. This was the mode used in collecting all TXR data discussed in this paper. (In chamber mode the entire TXR cryostat is contained in a host cryogenic vaccum chamber, and the TXR cryostat case and window can be at any temperature between room temperature and 77 K.) As shown in Fig. 1, a large black-painted baffle plate, called the scene plate, is located between the TXR cryostat and the blackbody under test and is used to block scattered light from the shiny TXR cryostat metal surfaces that could otherwise load the blackbody with uncontrolled background.

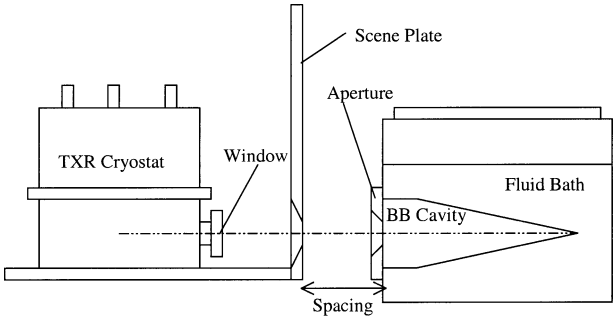

FIG. 1. The TXR as used during the Miami2001 intercomparison. The BB under test is depicted on the right and the spacing is close enough that the TXR pupil is overfilled by the BB.

The TXR had been deployed in chamber mode once prior to Miami2001 (Rice et al. 2003, 2000) and twice in chamber mode since Miami2001 (Manuscripts in preparation). After its initial chamber deployment test in 1999, the TXR itself was upgraded in January 2001 by adding an onboard blackbody system, increasing the gain of the channel 2 preamplifier, and reducing the full field of view to 30 mrad.

The complete calibration of the TXR includes system-level characterizations at a number of NIST facilities. Some measurements of its basic spectral, spatial, and temporal characteristics in ambient mode were reported previously (Rice and Johnson 1998). It is sufficient for the purposes of the Miami2001 intercomparison to consider only the calibration of the TXR against the radiance scale realized on the NIST WBBB. To assess repeatability and reproducibility, the TXR has been calibrated several times against the WBBB before and after Miami2001, and the calibration measurements were even performed once at Miami2001 as described in the next section.

The TXR was placed sufficiently close to each BB under test such that the TXR 30-mrad field of view was overfilled by the BB aperture. An internal red diode laser inside of the TXR, projected onto a sheet of graph

paper placed against the BB aperture during alignment, indicated the location of the radiometric center of the TXR field of view. The slight offset between this laser spot and the radiometric center of the TXR field of view had been determined by scanning the TXR across the WBBB at NIST prior to Miami2001, and this offset was applied when aligning the TXR at the geometric center of the apertures of all BBs that it measured at Miami2001.

4. TXR calibration against the NIST water bath blackbody

The TXR brightness temperature data in this paper were calibrated from raw TXR signals using data from an overnight calibration of the TXR against the NIST WBBB during Miami2001 on the evening of 31 May 2001. The TXR calibration consisted of measurements of the TXR response from channel 1 (InSb detector, filter centered at 5 μm) and channel 2 (MCT detector, filter centered at 10 μm) at a series of WBBB temperature setpoints, as shown in Fig. 2a. The WBBB nominal setpoints ranged from 20° to 60°C with a nominal spacing of 5° below 45°C and 2.5° above 45°C. These data were obtained using the following computer-automated procedure. Proceeding from lowest temperature to highest, the WBBB was first allowed to equilibrate at each temperature plateau. At each equilibrated temperature plateau, 100 stable readings of (a) the WBBB contact temperature as measured by the PRT, represented by the symbol T; (b) the TXR channel 1 response defined as the output of the channel 1 lock-in amplifier, represented by the symbol r_1; (c) the TXR channel 2 response defined as the output of the channel 2 lock-in amplifier, represented by the symbol r_2; and (d) the TXR chopper amplitude signal were simultaneously recorded. The TXR data were each measured by separate lock-in amplifiers having time constants of 1 s, and the 100 readings were taken approximately 2 s apart from each other. The 4-cm-diameter aperture was in place on the NIST WBBB during this calibration. The measured spacing (along the optical axis) between the TXR scene plate and the WBBB aperture reference plane was 64 mm. The tuning fork chopper amplitude data were used to apply a very small correction to the TXR signals that only becomes significant when the chopper amplitude drifts away from the value used during calibration. Occasional adjustment of the amplitude during the deployment and correction for the residual rendered this effect insignificant.

These TXR response calibration data of Fig. 2a were fit to an interpolating function

$$r_i(T) = a_i B(\lambda_i, T) + b_i, \tag{1}$$

where the subscript i represents the TXR channel number ($i = 1, 2$), $\lambda_1 = 5$ μm, $\lambda_2 = 10$ μm, a_i and b_i are parameters that are to be varied to obtain a good fit to the calibration data, and $B(\lambda_i, T)$ represents the Planck function at fixed wavelength,

$$B(\lambda_i, T) = \frac{c_1}{\lambda_i^5[\exp(c_2/\lambda_i T) - 1]}, \tag{2}$$

where $c_1 = 1.191066 \times 10^4$ W cm^{-2} sr^{-1} μm^4 and $c_2 = 1.43883 \times 10^4$ μm K, λ_i is in micrometers, and T is in degrees kelvin. The solid lines in Fig. 2a show the resulting best fit for each channel. The residuals (data − fit) of these calibration fits, shown in Fig. 2b, are within about ±30 mK for channel 2 (10-μm channel) and ±10 mK for channel 1 (5-μm channel). These are

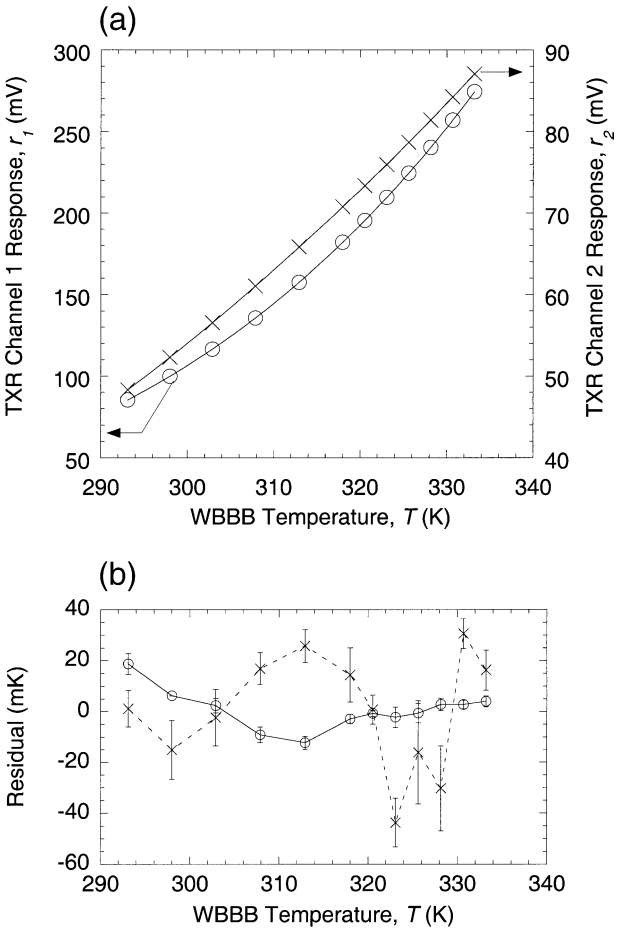

FIG. 2. (a) Calibration of TXR channel 1 and channel 2 signals vs WBBB SPRT temperature (T) at temperature plateaus during an overnight calibration at RSMAS, showing the best fits to the interpolating functions defined by Eq. (1) with parameters listed in Table 2. For each temperature plateau, the mean values of 100 successive samples are plotted as symbols (channel 1, O; channel 2, ×), and the fits to the interpolating functions are shown as solid lines. Error bars representing the std dev of repeated measurements at each plateau are too small to be seen on this scale. The 4-cm-diameter aperture was on the WBBB during this calibration. (b) Residuals (mean value − fit value) of the fit of the interpolating function to the TXR calibration data. The symbols indicate the residual value for each plateau (channel 1, O; channel 2, ×), and the error bars represent the std dev of the 100-sample populations collected at each plateau. The lines are guides for the eye.

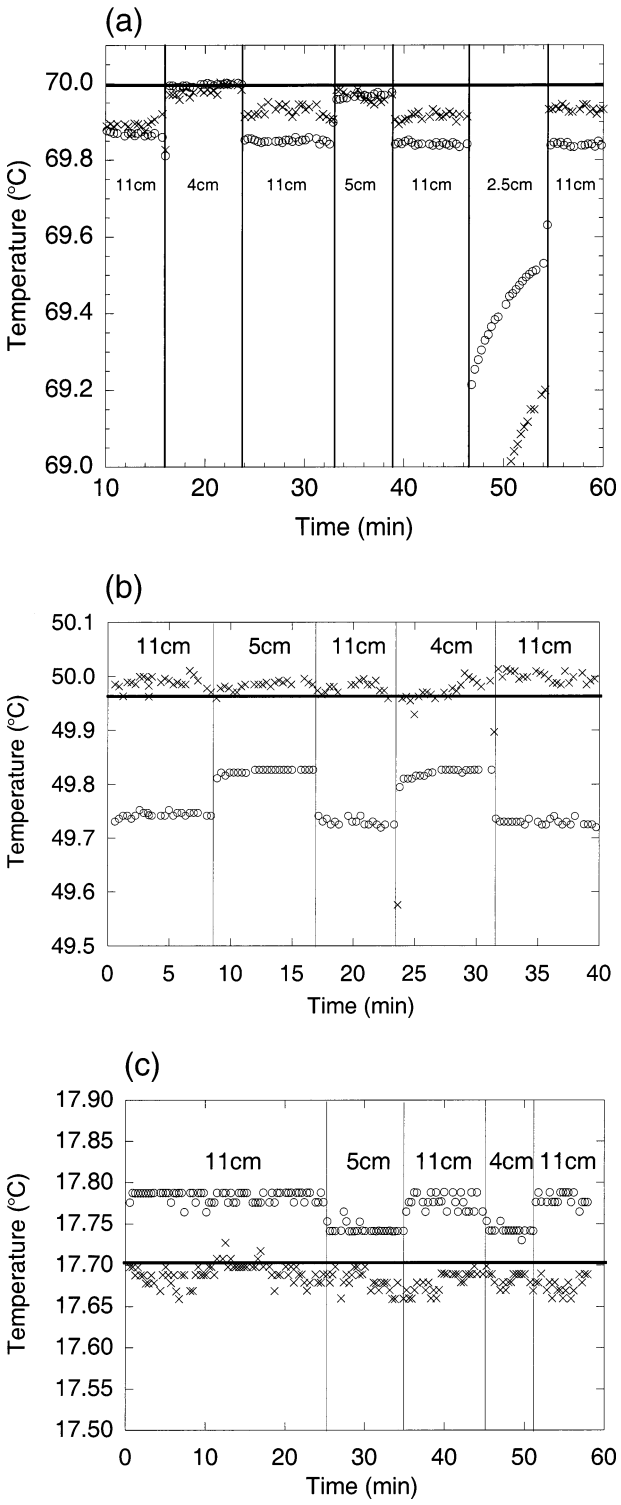

FIG. 3. Aperture reduction tests. The symbols are individual samples of the TXR-measured brightness temperatures (channel 1, 5 μm, O; channel 2, 10 μm, $\times$). The vertical lines (and data points falling near the vertical lines resulting from a temporary blocking of the TXR view while the aperture was being inserted or removed) indicate times when the aperture was inserted or removed. The aperture diameters during a given interval are indicated between the vertical lines. For clarity, only every 10th data point is shown: (a) NIST WBBB at 70°C (indicated by the horizontal line), (b) RSMAS BB at T_c = 49.964°C (indicated by the horizontal line), and (c) RSMAS BB at T_c = 17.705°C (indicated by the horizontal line).

TABLE 2. TXR calibration parameters derived from WBBB measurements and used during the Miami2001 intercomparison.

TXR channel i	λ_i (μm)	a_i (mV cm^2 sr μm W^{-1})	b_i (mV)
1	5	4.0271×10^5	1.7259
2	10	5.3567×10^4	0.87246

typical for TXR calibrations against the NIST WBBB in this temperature range (Rice and Johnson 1998). The error bars in Fig. 2b are only the contribution from the standard deviation of the time series of 100 readings for each channel. The best-fit parameters a_i and b_i listed in Table 2, are used in Eq. (1) for all subsequent conversions between temperature and r_i in this paper. Therefore, the calibration applied is relative to the NIST WBBB using the 4-cm aperture. Given a measured TXR response r_i(BBX) from any other blackbody, labeled BBX, at contact temperature T_c, the brightness temperature T_{bi} is then computed using the inverse of the interpolating function:

$$T_{bi} = \frac{c_2}{\lambda_i \ln\left\{\dfrac{c_1 a_i}{\lambda_i^5 [r_i(\mathrm{BBX}) - b_i]} + 1\right\}}, \qquad (3)$$

which was derived simply by solving Eq. (2) for T.

5. Aperture reduction tests

The blackbodies intercompared at Miami2001 were designed so that the emissivity is as high as possible even with a relatively large aperture diameter of about 10–11 cm. The TXR target spot diameter was about 3 cm, so it underviewed these apertures and enabled aperture reduction tests. In such tests, the brightness temperature is measured as a function of BB exit aperture diameter. For diameters between 3 and 11 cm, ideally there would be no dependence. We compared two of the BBs, the NIST and the RSMAS, in their performance in aperture reduction tests, and indeed found a dependence that can be explained by a full-aperture emissivity of slightly less than unity. Before describing the comparison of all BBs at full apertures in the following sections, we devote a bit of discussion here to these aperture reduction tests.

Typical data are shown in Fig. 3a. For this time series, which was measured at NIST several months after the Miami2001 intercomparison, the TXR was viewing the WBBB at a contact temperature of 70°C. The exit aperture of the WBBB, nominally 11 cm with no reduction

aperture, was reduced to 4 cm at a time of 16 min, returned to 11 cm at 24 min, reduced to 5 cm at 33 min, returned to 11 cm at 39 min, reduced to 2.5 cm at 46 min, and finally returned to 11 cm at 54 min. The reduction to either 5, 4, or 2.5 cm was performed by quickly (within 5 s) adding one of three appropriately sized reducing apertures onto the cavity. The TXR underviewed the 11, 5, and 4-cm aperture diameters, but not the 2.5-cm-diameter aperture. This can be seen in Fig. 3a, where the addition of the 2.5-cm aperture, initially at room temperature, cuts the TXR field of view enough that the heating of the aperture metal can be seen as a slow rise in brightness temperature during the time that the aperture is in place.

The reducing apertures are gold plated on the side facing the BB cavity, which would tend to increase the emissivity of the cavity. This increase, being optical rather than thermal, should occur instantly and result in an increase of the measured brightness temperature. This is indeed seen in the data of Fig. 3a. When either the 4- or 5-cm aperture is used, there is about a 0.15°C increase at 5 μm and a 0.1°C increase at 10 μm. Note that the effect is slightly larger for the 4-cm aperture. Since the 4-cm aperture gives the largest effective cavity emissivity without cutting the TXR field of view, it was used for the calibration of the TXR against the WBBB described in section 4.

Aperture reduction tests at Miami2001 were performed with the TXR viewing the RSMAS BB at 49.964°C on 31 May 2001 and the time series of the calibrated brightness temperature data, using the calibration coefficients of Table 2, are shown in Fig. 3b. During this time series, the 11-cm exit aperture of the BB was reduced to 5 cm at 7 min, returned to 11 cm at 17 min, reduced to 4 cm at 23 min, and returned to 11 cm at 31 min.

There are three important aspects of the data in Fig. 3b. The first is that the 5-μm data show that the reduction of the exit aperture of the RSMAS blackbody using either of these apertures causes an increase of brightness temperature of some 0.08°C, followed by a more gradual increase of another 0.01°–0.02°C. A plausible explanation for the instant effect is that it is the expected increase of the emissivity of the cavity, which is also seen with the NIST WBBB. The smaller, more gradual effect is presumed to result from changes of temperature gradients within the cavity and is insignificant. Given this explanation for the instant aperture reduction effect, the second, and potentially most interesting, aspect of the data is the lack of such an aperture reduction effect in the 10-μm data and the relatively good agreement between brightness temperature and contact temperature. This is a useful result for the RSMAS blackbody, as it appears (within this model) that at 10-μm the emissivity at 49.964°C is not increased upon reduction of the aperture, which is the ideal case. The third important aspect of the data is that even with the 4-cm-diameter aperture, the 5-μm brightness temperature is nearly 0.15°C below the contact temperature.

A probable explanation for the third aspect is that the TXR 5-μm channel drifted out of calibration by 0.15°C due to humidity changes in the laboratory at RSMAS between its overnight calibration against the NIST WBBB and its daytime use for the RSMAS BB measurements. The bandpass of the 5-μm channel, extending from 4.5 to 5.5 μm, encompasses a number of water vapor absorption lines, particularly in the region from 5.0 to 5.5 μm. The two effects of water vapor were estimated by numerically integrating the product of the Planck blackbody spectrum and the water vapor transmittance spectrum over the bandpass. One effect is absorbance through the 0.5-m pathlength from the BB cavity to the TXR window. The other competing effect is the additional radiance measured from emission of water vapor (near-ambient temperature) along the same pathlength. The total estimated effect for a BB at 50°C is a decrease of 0.033% in the measured band-integrated radiance for each percent of relative humidity increase. Thus the change of measured brightness temperature of −0.15°C, corresponding to a change of measured band-integrated radiance of 0.47%, could be accounted for by an increase of 14% in the relative humidity in the laboratory between nighttime calibration and daytime use. This is a reasonable change that could have occurred. The 10-μm channel does not suffer from this effect, as there are not significant water vapor lines in its bandpass. Note that the TXR was designed primarily for vacuum use, where water vapor absorption does not exist, and that the bandpass of the 5-μm channel was optimized for other effects rather than complete immunity to water vapor. It can be concluded that while the channel 2 (10 μm) data are useful for blackbody intercomparisons even in the presence of humidity changes, the channel 1 (5 μm) data are not. Thus only the channel 2 data are used for detailed analysis below.

Figure 3c shows the aperture test with the RSMAS blackbody at 17.705°C, the only other temperature where it was performed. Note that the ambient temperature was about 26°C. The reduction of the aperture diameter now causes an instant reduction in the 5-μm brightness temperature, as one would expect from the emissivity explanation when applied to a blackbody below ambient temperature. Also, the 5-μm brightness temperature, even with the 4-cm aperture on the RSMAS BB, is 0.05°C higher than T_c, whereas the 10-μm brightness temperature agrees to within its uncertainty. This is consistent with the humidity effect on the 5-μm channel described above, since with the BB cavity below ambient temperature the emitted radiance from the ambient water vapor in the path dominates the loss of BB cavity radiance from water vapor absorbance, such that the net effect is to increase the measured brightness temperature.

TABLE 3. Results of temperature sweeps. Extraction of 10-μm relative effective emissivity from ΔL_2 plots in Fig. 6. The slope of each ΔL_2 plot in Fig. 6 gives $1 - \varepsilon_{BBX}$ and the intercept gives $(1 - \varepsilon_{BBS})B(\lambda_2, T_s)$ as indicated in Eq. (7). This enables a determination of values for the 10-μm relative effective emissivity, shown in boldface. The fitting uncertainties are tabulated with $k = 1$ (1σ). For reference, the first row gives values for direct measurements of the spacing (along the optical axis) between the TXR sceneplate and the blackbody aperture reference plane.

Quantity	RSMAS BB	JPL BB	CASOTS RAL BB
Spacing (mm)	64	128	114
$1 - \varepsilon_{BBX}$	1×10^{-5}	8.379×10^{-3}	9.457×10^{-3}
$1 - \varepsilon_{BBX}$ fitting uncertainty	7×10^{-4}	8.43×10^{-4}	6.44×10^{-4}
ε_{BBX}	**1.0000**	**0.9916**	**0.9905**
ε_{BBX} fitting uncertainty	**0.0007**	**0.0008**	**0.0006**
Intercept (W cm^{-2} sr^{-1})	-1.9×10^{-7}	-8.96×10^{-6}	-1.047×10^{-5}
Intercept fitting uncertainty (W cm^{-2} sr^{-1})	8×10^{-7}	9.4×10^{-7}	7.2×10^{-7}
T_s (°C)	N/A	31.57	33.82
T_s fitting uncertainty (°C)	N/A	0.28	0.05

6. Temperature sweeps

The major measurement activity during the laboratory intercomparison was having the TXR view each participating blackbody as its temperature was swept across a broad range likely to be encountered during use. For each of these tests, the TXR was aligned to the geometrical center of the participating blackbody. Since the goal was to measure each blackbody in the way it is normally used to calibrate sea surface temperature radiometers, no reducing apertures were applied. The TXR scene plate was in place for all tests, as shown in Fig. 1, providing a black surround with monitored temperature as the scene viewed by each blackbody under test. The spacing between the TXR scene plate and the front of each participating BB is noted in Table 3. During the entire temperature sweep of each BB, the TXR computer logged (a) the TXR channel 1 response, r_1, defined as the output of the channel 1 lock-in amplifier; (b) the TXR channel 2 response, r_2, defined as the output of the channel 2 lock-in amplifier; and (c) the TXR chopper amplitude signal. The TXR data were each measured by separate lock-in amplifiers having time constants of 1 s, and the 100 readings were taken approximately 2 s apart from each other. After each 100-reading interval, averages and standard deviations of the interval were logged along with TXR environmental temperatures and laboratory humidity and pressure. Simultaneously, using a separate computer for datalogging, the contact temperature, T_c, of each participating blackbody was measured using a thermometer in the blackbody fluid bath. Participants were notified that the thermometer, its location, and everything else about the operation of their blackbody should, to the extent possible, simulate the way their equipment is operated during actual calibration of their radiometers.

Collecting data in this way required that at a later time, during a postexperiment analysis phase, each TXR data file had to be combined with the appropriate T_c data file. The combination involved correcting for slight errors in the time synchronization of the datalogging computer clocks and, since the data were not necessarily collected at the same sampling frequency, resampling each time series to ensure near-simultaneous data sampling between the blackbody temperature (T_c) and the TXR responses (r_i). As the sampling rates ranged from once per 1 s to once per 4 s, the greatest degree of nonsimultaneity was at about 2 s. This is considered negligible, given the relatively long thermal time constants of the participating blackbodies.

The warming profiles in Fig. 4 show that the participating blackbodies were each swept through a series of temperature plateaus, similar to the way the WBBB was used (section 4) to calibrate the TXR. Here, however, the blackbodies were operated manually. The RSMAS fluid bath blackbody was allowed to stabilize to equilibrium at each plateau, and, because of its active temperature control, the bath temperature did not drift. It has an internal refrigerator to enable reaching the lowest temperatures, and it was set to successively higher temperature plateaus by increasing the setpoint temperature of its active controller at the end of each plateau. The water cooler blackbodies (JPL, CASOTS RAL, and CASOTS SOC) have no provision for active temperature control, so the bath temperature for each tended to drift slightly even on the plateaus. They were cooled to the lowest temperatures by adding ice to the water bath, and warmed to successively higher temperatures by using an electrical heater inserted into the bath for a short time. A high-volume water pump was also inserted in to the water baths to keep the water temperature as uniform as possible. Their lids were closed during the plateaus in order to provide the greatest degree of thermal isolation of the bath from the surroundings.

7. Results and analysis

Figure 5 shows the results of the intercomparison in terms of 10-μm TXR brightness temperature (T_{b2}) minus contact temperature (T_c) for all four participating blackbodies: RSMAS BB, JPL BB, CASOTS RAL BB, and CASOTS SOC BB. The T_c values for each BB are

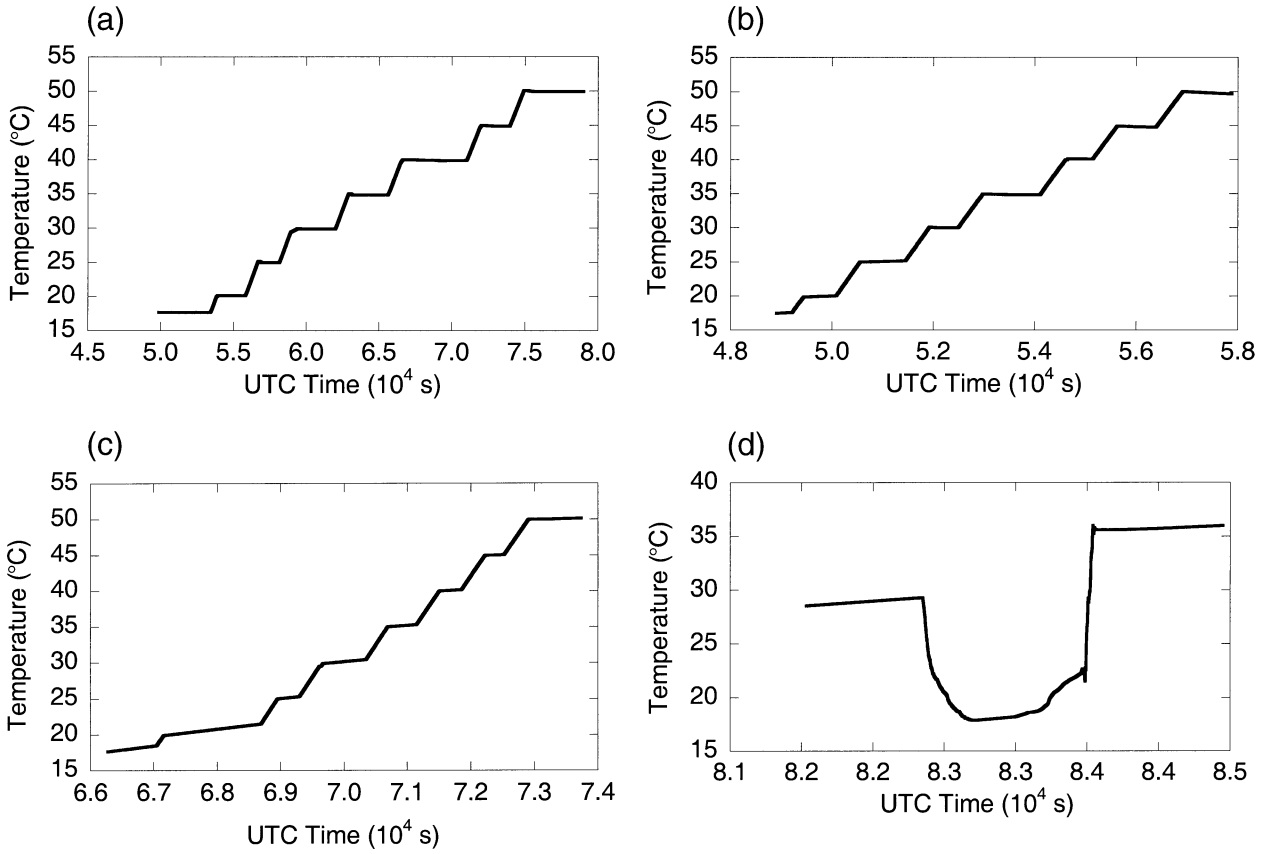

FIG. 4. Contact temperature (T_c) vs time data for each of the blackbodies tested. The temperature sweeps were from lowest to highest temperature. On this scale, brightness temperature data taken simultaneously in both channels of the TXR lay on top of the contact temperature and are not plotted. Only data near the end of each plateau were used for the analysis as described in section 7: (a) RSMAS blackbody, (b) JPL blackbody, (c) CASOTS RAL blackbody, and (d) CASOTS SOC blackbody.

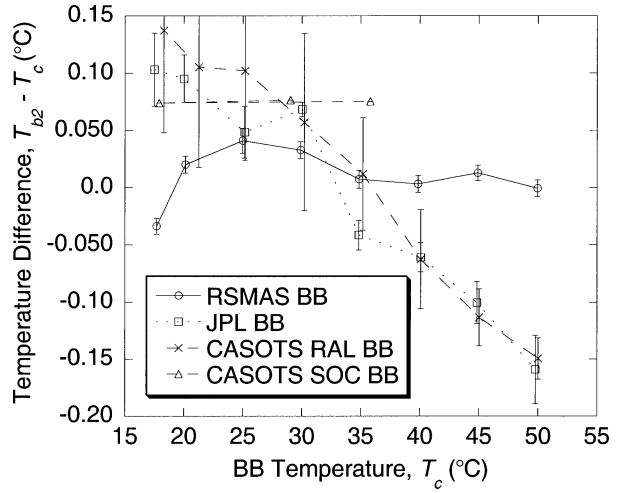

FIG. 5. Comparisons of 10-μm brightness temperatures from the temperature sweep measurements, using Eq. (3) to convert the measured TXR response to brightness temperature with the calibration coefficients in Table 2. The symbols are from the mean values of data points (spaced every 2 s) averaged over the last 100 s of each plateau (except for the CASOTS SOC BB, where only the last value of each plateau is plotted). The error bars are the std dev of the values over this time interval. The lines are guides for the eye.

from the user's choice of thermometer placed in the BB water bath. Averages over the last 200 s of each plateau interval are reported for all but the CASOTS SOC comparison, and the error bars represent the standard deviation of the 100 readings of this last, most stable interval on the plateau. The RSMAS BB error bars are much lower, down at the stability level of the TXR, since the RSMAS BB was under active temperature control and so its plateaus were very flat with time. For the other blackbodies, the lack of active temperature control over the plateau caused temperature drift to dominate the uncertainty, hence the larger error bars. Plotting only instantaneous points, rather than interval averages, gives similar results.

Figure 5 shows that the RSMAS BB 10-μm brightness temperature agrees with that of the NIST WBBB over the entire range of temperatures studied, to within the ± 0.05°C ($k = 2$) uncertainty of the TXR. It also shows that the JPL BB and the CASOTS RAL BB agree with the NIST WBBB this well only near 30°C, giving too high a value at lower temperatures and too low a value at higher temperatures. Given that the surrounding ambient temperature was near 30°C, this indicates that

these blackbodies have effective emissivities significantly less than unity.

This can be analyzed by considering that the radiance seen by the radiometer is the sum of the radiance emitted by the blackbody itself at temperature T_c and that emitted by the surroundings at temperature T_s and reflected from the blackbody:

$$L_i(\text{BBX}) = \varepsilon_{\text{BBX}} B(\lambda_i, T_c) + (1 - \varepsilon_{\text{BBX}}) B(\lambda_i, T_s), \quad (4)$$

where L_i(BBX) and ε_{BBX} are, respectively, the radiance and relative effective emissivity of the blackbody under test. Here the first term represents emitted radiance and the second represents reflected radiance. Using the WBBB with a 4-cm aperture as the reference is equivalent to assuming that its effective emissivity is close enough to unity that the reflected radiance term cannot be seen by the TXR. This is equivalent to making the approximation $\varepsilon_{\text{WBBB}} = 1$ and then ε_{BBX} is the effective emissivity of BBX relative to that of the WBBB. That is, a BB that had identical emissivity to that of the WBBB would give radiance

$$L_i(\text{WBBB}) = B(\lambda_i, T_c). \quad (5)$$

Remember that the TXR response to any blackbody can easily be converted to total band-integrated radiance seen by the TXR through the interpolating function defined earlier:

$$L_i = \frac{r_i - b_i}{a_i}. \quad (6)$$

Thus the radiance values on the left-hand side of Eqs. (4) and (5) are actually directly from TXR measurements. Subtracting Eq. (4) from Eq. (5), one expects the difference of the TXR radiance measurements to follow:

$$\Delta L_i \equiv L_i(\text{WBBB}) - L_i(\text{BBX})$$
$$= (1 - \varepsilon_{\text{BBX}}) B(\lambda_i, T_c) - (1 - \varepsilon_{\text{BBX}}) B(\lambda_i, T_s), \quad (7)$$

where the first term on the right-hand side increases with T_c and the second term does not. Thus a plot of ΔL_2 versus $B(\lambda_2, T_c)$ for each BBX should give a straight line with slope $(1 - \varepsilon_{\text{BBX}})$ and a negative intercept of magnitude $(1 - \varepsilon_{\text{BBX}}) B(\lambda_2, T_s)$. Figure 6 shows such plots for three of the participating blackbodies, and Table 3 gives the corresponding parameters resulting from linear fits along with values of ε_{BBX} and T_s extracted from the parameters. For the RSMAS BB, the relative emissivity is the same as that for the WBBB to within the uncertainty. For both the JPL BB and CASOTS RAL BB, the model fits well with relative effective emissivity of about 0.991 at 10 μm for each BB. We suspect that the reduced emissivity of these BBs may have resulted from the accumulation of dust or other types of contamination in the cavities that result from using them in harsh conditions.

The values for T_s extracted from the intercepts of the plots are near 33°C. Two ambient thermometers, calibrated to within ±1°C, one in contact with the TXR scene plate and the other in the room, indicated that ambient temperature ranged from 25° to 26°C during the measurements. Here, T_s represents this ambient temperature in the model, and its extracted values are within about 8°C of these more direct thermometer measurements. That the difference is greater than the T_s fitting uncertainty indicates that there are other sources of uncertainty in applying the model at this level of detail that have not been quantified. Considering the simplicity of the model, the ability to extract the ambient temperature to within 8°C from reflected radiance measurements of blackbodies gives further confidence in the measurements and the model.

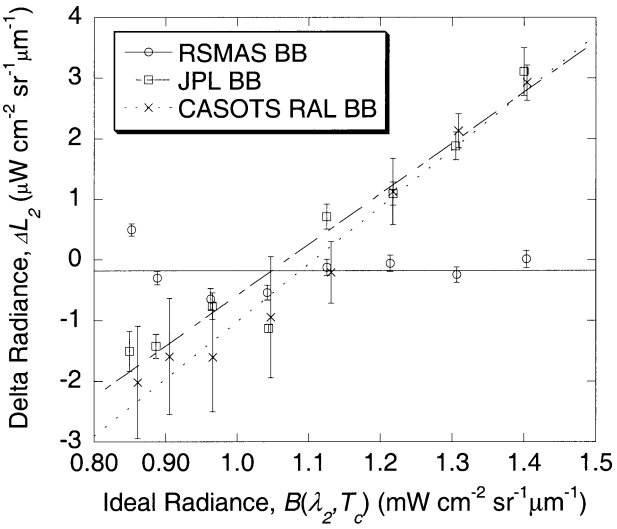

FIG. 6. Comparisons of 10-μm radiance, enabling extraction of relative emissivity. Delta radiance is defined in Eq. (7), and ideal radiance is defined by the Planck function, Eq. (2). The symbols are calculated from the mean (over the last 100 points of each temperature plateau) TXR response to BBX using Eq. (6), and the error bars are the std devs of those values. The lines are the best fits of Eq. (7) to the data for each blackbody, corresponding to the values of the parameters listed in Table 3.

The calculated absolute emissivity of the NIST WBBB was 0.9997 ± 0.0003 without a reducing aperture, and with a 5-cm-diameter aperture it was calculated to increase to 0.99997 ± 0.00003 (Fowler 1995). From the data described in section 4 and plotted in Fig. 3a, the observed 10-μm channel brightness temperature increase between the 11- and the 5-cm aperture cases is 0.051 ± 0.017 K. This corresponds to a radiance increase of 0.063% ± 0.020%, resulting from an absolute emissivity increase of 0.00063 ± 0.00020. This observed emissivity increase agrees with the calculated emissivity increase (0.00027 ± 0.00030) to within the mutual uncertainty ($k = 1$) values, giving some confidence in the calculated absolute emissivity values. The philosophy of the comparison reported here was therefore to use the NIST WBBB with the 4-cm aperture, which gives the WBBB an even higher emissivity than the 5-cm aperture, and measure all other blackbodies

relative to it. While a calculation of the emissivity of the NIST WBBB with the 4-cm aperture has not been performed, the value would be bounded from above by unity and below by the calculated value for the 5-cm aperture of 0.99997 ± 0.00003.

8. Conclusions

The agreement between the NIST water bath blackbody with a 4-cm aperture and the RSMAS blackbody at any aperture diameter as verified by the TXR 10-μm channel is within the noise and fitting uncertainty (about ±50 mK, $k = 2$) of the data. The 5-μm data do not agree well because the TXR 5-μm channel is influenced slightly by water vapor absorption. The CASOTS RAL and JPL blackbodies do not agree at temperatures away from ambient, although they do agree to within ±0.1°C as long as they are near ambient. Effective emissivity values relative to the NIST water bath blackbody were near 0.991 at 10 μm for both of these blackbodies. The CASOTS SOC blackbody was not measured carefully enough to draw any definite conclusions. Careful use of these blackbody targets to calibrate ship-based radiometers used in the validation of satellite-derived skin sea surface temperatures could therefore result in validation datasets that have uncertainties within ±0.1°C. This intercomparison also demonstrates some of the verification capabilities that are now available to the environmental remote sensing community with the use of the NIST TXR.

Acknowledgments. Funding to support the Miami2001 workshop was made available by three members of the international Committee on Earth Observation Satellites (CEOS): EUMETSAT, NOAA/NESDIS, and ESA. These contributions to ensure the success of the laboratory and ship campaigns are gratefully acknowledged. The support for travel and other expenses by all participants' institutes or other funding agencies is also acknowledged. In particular, the TXR development and its deployment at Miami2001 were funded in part by the NASA EOS Project Science Office. The research described in this paper was carried out in part at the Jet Propulsion Laboratory, California Institute of Technology, under a contract with NASA as part of the EOS Mission to Planet Earth.

REFERENCES

Barton, I. J., P. J. Minnett, K. A. Maillet, C. J. Donlon, S. J. Hook, A. T. Jessup, and T. J. Nightingale, 2004: The Miami2001 infrared radiometer calibration and intercomparison. Part II: Shipboard results. *J. Atmos. Oceanic Technol.*, **21,** 268–283.

Donlon, C. J., T. Nightingale, L. Fiedler, G. Fisher, D. Baldwin, and I. S. Robinson, 1999: The calibration and intercalibration of seagoing infrared radiometer systems using a low cost blackbody cavity. *J. Atmos. Oceanic Technol.*, **16,** 1183–1197.

Fowler, J. B., 1995: A third generation water bath based blackbody source. *J. Res. NIST*, **100,** 591–599.

Rice, J. P., and B. C. Johnson, 1998: The NIST EOS thermal-infrared transfer radiometer. *Metrologia,* **35,** 505–509.

——, S. C. Bender, and W. H. Atkins, 2000: Thermal-infrared scale verifications at 10 micrometers using the NIST EOS TXR. *Proc. SPIE,* **4135,** 96–107.

——, S. C. Bender, W. H. Atkins, and F. J. Lovas, 2003: Deployment test of the NIST EOS thermal-infrared transfer radiometer. *Int. J. Remote Sens.*, **24,** 367–388.